Nuclear Inst. and Methods in Physics Research, A 928 (2019) 51–57

Contents lists available at ScienceDirect

Nuclear Inst. and Methods in Physics Research, A

journal homepage: www.elsevier.com/locate/nima

Neutron–gamma discrimination based on quantum clustering technique

Y. Lotfi [a], S.A. Moussavi-Zarandi [a,*], N. Ghal-Eh [b,c], E. Pourjafarabadi [d], E. Bayat [e]

[a] Department of Energy Engineering and Physics, Amir Kabir University of Technology, P.O. Box 15875-4413, Tehran, Iran
[b] School of Physics, Damghan University, P.O. Box 36716-41167, Damghan, Iran
[c] Department of Physics, School of Sciences, Ferdowsi University of Mashhad, P.O. Box 91775-1436, Mashhad, Iran
[d] Physics Department, College of Sciences, Shiraz University, P.O. Box 71454, Shiraz, Iran
[e] Nuclear Science and Technology Research Center, AEOI, P.O. Box 14155-1339, Tehran, Iran

ARTICLE INFO

Keywords:
Digital pulse shape discrimination
FoM
Liquid scintillator (BC501)
Quantum clustering

ABSTRACT

In this study, the digital neutron–gamma discrimination (DNGD) has been undertaken based on the pulse-shape discrimination on the anode pulse of a 2" by 2" right cylinder BC501A liquid scintillator with a fast data acquisition card (14-bit resolution, 500 MS/s). Seven different features of the anode pulse have been extracted and the discrimination based on quantum clustering (DBQC) has been studied. The influence of three different parameters (*i.e.*, η, σ and K) on the discrimination figure-of-merit (FoM) has been investigated. In addition, the FoM dependencies on different choices of DBQC features have been determined. A 100 mCi ^{241}Am-Be neutron source has been used for the DNGD and the calibration has been made with a 1.1 μCi ^{22}Na gamma-ray source. The results show that the FoM value is around 1 at 100 keVee bias energy, whilst this value can be improved up to 50% by choosing and setting appropriate features.

1. Introduction

Neutron sources are always accompanied by the de-excitation gamma rays whose discrimination from neutrons is basically a complicated task [1]. Both analog and digital techniques can be used for such discrimination with BC501A (or its equivalent, NE213) scintillator [2]. The main advantages of DNGD are software-controllability and simple-installation. The zero-cross, time-of-flight and Owen are the most famous methods introduced in the 1970's [3]. In DNGD, on the other hand, the anode pulses of the scintillator are sampled with the digitizer before they are processed. The DNGD is generally discussed in two different categories. In some studies, the important parameters of digitizers have been investigated in order to improve the NGD quality [4–7]. Whilst, some studies focus on the low-resolution digitizers incorporating some software techniques for the NGD improvement [8, 9].

In recent years, numerous digital methods have been introduced for the NGD analysis, such as pattern reorganization method (PRM) [10], artificial neural networks (ANN) [11], charge integration method (CIM), frequency gradient analysis method (FGAM), wavelet packet transform method (WPTM) [12] and discrete Fourier transform method (DFTM) [13].

The main problem associated with the NGD is that at low neutron energies, a very small amount of scintillation light is produced in the cell, which results in very small pulse-height and, consequently, small signal-to-noise ratio and discrimination FoM. In the present study, to resolve this problem, the quantum clustering algorithm (QCA) has been proposed, which was previously used in the segmentation of satellite images [14], the identification of hidden radioactive source in a city region [15], medical imaging [16–18] and so on.

In DNGD, output pulses of the scintillation detector, which are a mixture of both neutron and gamma ray pulses, are logged by a digitizer. In clustering, the detector pulses of more similar properties are classified into separate groups in order to perform on the NGD, which has to be undertaken in terms of some specific pulse features. Then, the clustering is performed using software methods.

In this study, an innovative method based on data clustering technique (DBQC) is proposed for the DNGD. The DBQC is an unsupervised method [19] in which the data classification is undertaken in terms of their density fluctuations. In this method different parameters may be introduced for data classification. Since, in DBQC, there exist numerous parameters for the identifications of neutron and gamma ray pulses, the NGD quality is better improved especially in the low-energy region.

2. Materials and methods

2.1. Detection setup

A 2" by 2" right cylinder BC501A liquid scintillator has been used in the DNGD studies. The detector consists of a 1 mm thick aluminum scintillator cell and a borosilicate optical glass window. The photomultiplier tube (PMT) has been a 12-dynode HAMAMATSU R1828 with a linear-focused dynode structure and an appropriate μ-metal housing.

* Corresponding author.
E-mail address: moussavi.zarandi@gmail.com (S.A. Moussavi-Zarandi).

https://doi.org/10.1016/j.nima.2019.03.009
Received 4 February 2019; Received in revised form 25 February 2019; Accepted 3 March 2019
Available online 11 March 2019
0168-9002/

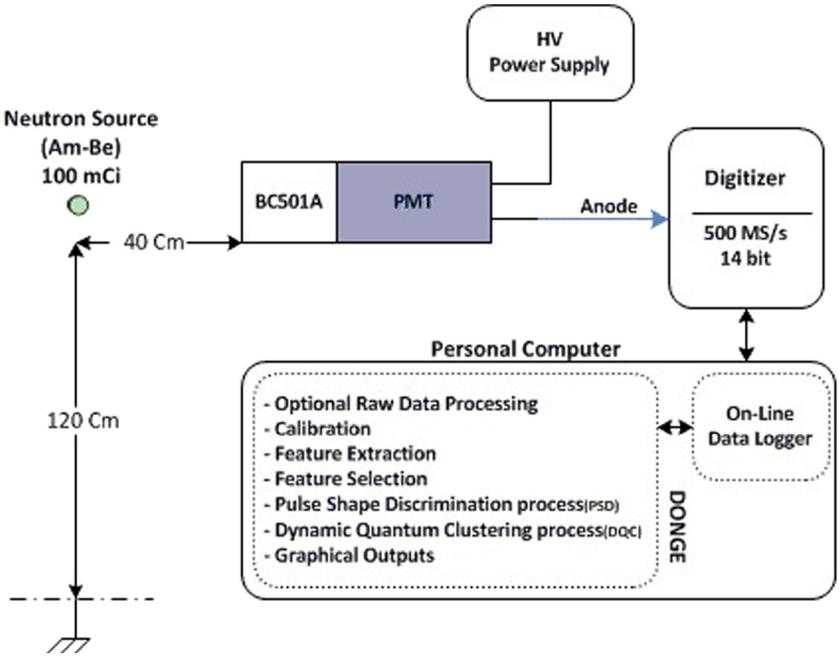

Fig. 1. The experimental setup used for DNGD.

In most NGD studies, the anode pulse is normally used to increase the through-put and to suppress the dead-time. The operating voltage has been -1600 V, and a 100 mCi ^{241}Am-Be neutron source has been used for DNGD. The calibration has been made on the Compton edge of 1.1 μCi ^{22}Na gamma-ray source, which is assumed to be located at 89% of descending edge of the spectrum [20]. In order to reduce the neutron scattering effects, both the detector and neutron source have been placed on a 120-cm high table top at 300 cm far from the surrounding walls (See Fig. 1).

2.2. Digitizer setup and feature extraction

The anode pulse of the BC501 scintillator has an exponential form (Fig. 2). The neutron and gamma ray interactions with liquid scintillator generally result in recoiled-protons and fast electrons generations, respectively. Since, the protons have much higher stopping power values than electrons as they travel inside the scintillator, the delayed fluorescence is different for these two particles. Hence, the output signals corresponding to protons represent longer decay times than those for electrons [1]. This difference is more enhanced in liquid scintillators, known as PSD, which is a unique property that can be used in the NGD.

The anode pulses of the detector have been captured with a USB-connecting digitizer card whose sampling rate and the resolution are 500 MS/s and 14 bits, respectively. A dedicated software, named DONGE (standing for Discrimination of Neutron and Gamma-ray Events), has been developed in LabView 2012 environment to perform different processions on the data taken from the digitizer for obtaining optimum NGD parameters. The DONGE flowchart is shown in Fig. 3.

In DONGE software, the captured pulses are recorded in a file. Then a specific number of pulses determined by the user are read to extract a few pulse features. As shown in Fig. 2, the anode pulses are divided into three different parts using three specific points namely, start point (StP), discrimination point (DsP) and stop point (SpP), as in the following: Long region (LR): It covers the whole pulse from StP to SpP. Short region (SR): The first region from StP to DsP. Discrimination region (DR): It includes the region from DsP to SpP. The extracted features are as follows:

(1) Long region integral (LRI): The pulse integration from StP to SpP.

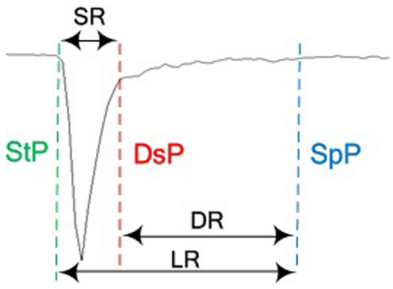

Fig. 2. The typical anode pulse of a BC501A scintillator.

(2) Short region integral (SRI): The pulse integration from StP to DsP.

(3) Discrimination region integral (DRI): The pulse integration from DsP to SpP.

(4) PSD: The fraction DRI/LRI.

(5) Pulse width (PW): The time difference between StP and SpP.

(6) Min value (MV): The minimum value of anode pulse.

(7) Discrimination index (DI): The time difference between StP and DsP.

In DONGE software, the PSD parameter is calculated for every anode pulse and the pulse features whose PSD is within 0 to 1 are stored in the buffer. Then, the PSD values are 3D-plotted against the NGD LRI as shown in Fig. 4.

2.3. The new PSD method

The DONGE software extracts seven different features from every detector pulse which are LRI, SRI, DRI, PSD, PW, MV and DI. In the common procedures, the NGD is undertaken based on the 3D plot of PSD against LRI. Since, at low neutron and gamma ray energies, the anode pulse-height is small and consequently the S/N reduces and the pulses are not well discriminated against PSD values. To resolve this problem, a new DBQC method is proposed to improve the NGD performance. The DBQC is based on the QC in which a d-dimensional Euclidean space is defined in terms of the d number of extracted

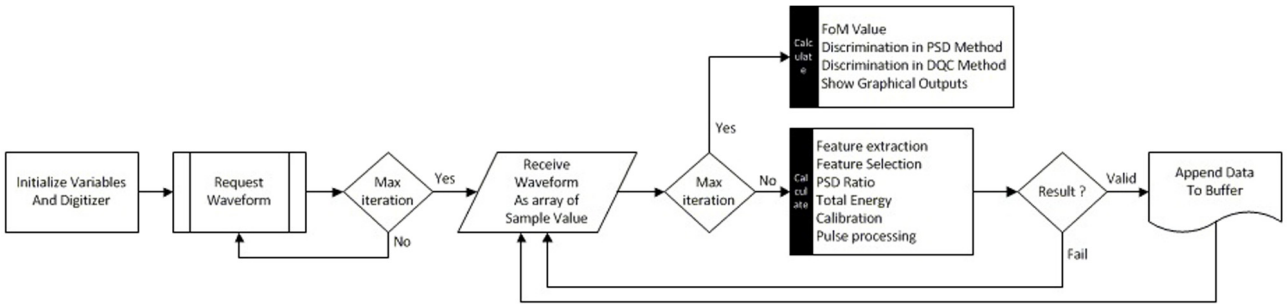

Fig. 3. The flowchart of DONGE software developed for pulse shape processing.

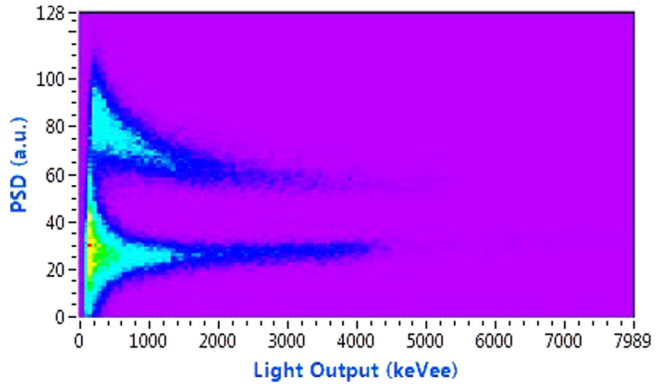

Fig. 4. A 3D NGD spectrum of BC501A scintillator when exposed ^{241}Am-Be source.

features from detector pulses. Every detector pulse is a point in the above mentioned space which is associated with a vector $\vec{x_i}$. Some of these points correspond to neutrons and some of them to gamma rays. The DBQC is an unsupervised [19] method in which the clustering is undertaken in terms of data density fluctuations. In this method, a Gaussian function is considered for every point as following:

$$\psi_i(\vec{x_i}) = e^{-\frac{(\vec{x}-\vec{x_i})^2}{2\sigma^2}} \tag{1}$$

where σ is a measure of Gaussian width. Therefore, the Gaussian distribution function for all points in d-dimensional space is:

$$\psi(\vec{x}) = \sum_i \psi_i(\vec{x_i}) = \sum_i e^{-\frac{(\vec{x}-\vec{x_i})^2}{2\sigma^2}} \tag{2}$$

This function has the local maxima at which regions in the feature space are more accumulated, hence; they can be used for data clustering. In some occasions, the maxima is not well-specified which results in incorrect clustering. In order to identify the number and the locations of maxima, one has to vary σ value which may slightly help. Alternatively, a more accurate and precise way to specify the maxima locations is to assume that ψ is an eigen state, with eigen value E, which applies to the following Schrödinger equation:

$$H\psi(\vec{x}) = (-\frac{\sigma^2}{2}\nabla^2 + V(x))\psi(\vec{x}) = E\psi(\vec{x}) \tag{3}$$

where V(x) is the potential function of position. The local minima of V(x) correspond to the maxima of ψ(x). However, the advantage of using V(x) instead of ψ(x) is that the minima of V(x) are more recognizable than the ψ(x) maxima [19]. Therefore, it has been decided to use the minima of V(x) in data clustering, which are called cluster centers (CC). All data points in the space need to be analyzed to determine to which CC they can be assigned in terms the feature similarities. To identify this similarity, one has to let the data points move as a result of potential, whose motion directions are normally towards the CCs. Despite existence of numerous CCs, the data points are attracted to the nearest or the most powerful CC, which results in an improved clustering. The gradient descent method (GDM) [21] is used for the motion of data points to the corresponding CCs where the effective force is $-\nabla V$, which pushes the data points to the nearest or the most powerful cluster center. The motion dynamics of data points is as follows:

$$x_{i_{new}} = x_i - \eta\nabla V(x_i) \tag{4}$$

The above equation shows that the data points at x_i with potential $V(x_i)$, move towards a CC by a force whose magnitude and direction are given by $-\nabla V$. The motion of data points occurs for all points in the space; as a result, the potential changes. In other words, all data points will have new potentials and the motion of data points will be towards the new potential minima. The data points density increases around the CC, so the clustering improves. The η is the step size value in GDM method, which has to be updated at every stage [22]. For the simplicity, the η value is assumed constant which is a correct assumption for small η's [23].

If the process of moving all data points towards the CC is called data time evolution (DTE), as the number of DTEs (K) increases, so do the data points density around the CC. Therefore, in QC method with the time evolution of data points following the GDM method, three parameters σ, η and K have to be determined and optimized according to the problem.

2.4. Implementation of new PSD method

The algorithm of DBQC has been developed in MATLAB R2014a. The steps undertaken in the algorithm are as the following:

(Step 1) Construction of input data matrix (IDM): If it is assumed that the n number of detector pulses are given, the m features of which have been extracted. In other words, for every detector pulse the data point x_i is written as following:

$$x_i = F_{i0}\hat{e}_0 + F_{i1}\hat{e}_1 + \cdots + F_{i(m-1)}\hat{e}_{(m-1)} \tag{5}$$

where the IDM is an $n\times m$ matrix which can be illustrated as:

$$IDM = \begin{bmatrix} F_{00} & F_{01} & \cdots & F_{0(m-1)} \\ \vdots & \vdots & \vdots & \vdots \\ F_{(n-1)0} & F_{(n-1)1} & \cdots & F_{(n-1)(m-1)} \end{bmatrix} \tag{6}$$

(Step 2) Selection of σ value and calculation of ψ(x): ψ(x) is so calculated for n points that it is a scalar for each point, therefore, it can be illustrated as $n\times 1$ matrix, viz.:

$$\psi(x) = \begin{bmatrix} \psi(x_0) \\ \vdots \\ \psi(x_{(n-1)}) \end{bmatrix} \tag{7}$$

(Step 3) The value of $\nabla V(x_i)$ for all data points are calculated as following:

$$\nabla V(x_i) = \frac{1}{2\sigma^2\psi^2(x)}[(-\sum_0^{n-1}(AB^2\frac{\overline{B}}{\sigma^2} + 2A\overline{B}))\psi(x) \tag{8}$$

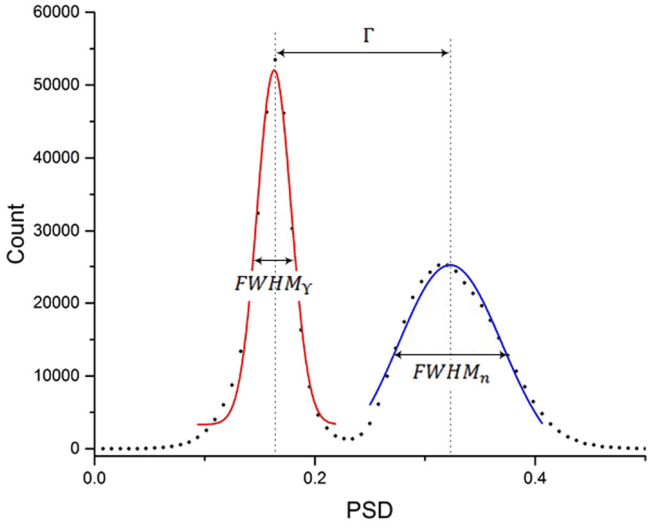

Fig. 5. 2D illustration of the NGD used for the definition of FoM.

$$- (\sum_{0}^{n-1} A\overrightarrow{B})(\sum_{0}^{n-1} AB^2)]$$

$$A = e^{-\frac{(\vec{x}-\vec{x_i})^2}{2\sigma^2}}$$

$$\overrightarrow{B} = (\vec{x} - \vec{x_i})$$

(Step 4) The motion of data points towards the CCs and the construction of output data matrix (ODM): At this stage, based on the selected η, the $x_{i_{new}}$ values following the Eq. (4), are calculated as the new x_i values. According to the motion of data points towards the CCs, the IDM values are updated and the ODM matrix is formed:

$$ODM = \begin{bmatrix} F'_{00} & F'_{01} & \cdots & F'_{0(m-1)} \\ \vdots & \vdots & \vdots & \vdots \\ F'_{(n-1)0} & F'_{(n-1)1} & \cdots & F'_{(n-1)(m-1)} \end{bmatrix} \quad (9)$$

(Step 5) Iteration: The values of initial matrix, IDM, are updated and the output matrix, ODM, is formed going through Steps 1 to 4. To improve the NGD, the ODM is as IDM and Steps 2 to 4 are repeated, where K is the number of iterations. The ODM data, after K iterations, are used for the NGD.

2.5. Figure of merit (FoM)

FoM is a measure of the NGD quality, which is defined as the separation of neutron and gamma ray peaks in the histogram plot of intensity versus PSD (See Fig. 5), following Eq. (10). The FoM value increases as the separation of neutron and gamma ray peaks increases, or/and the widths of neutron and gamma ray peaks decreases, which result in better NGD. In Section 3, the results are presented in terms of FoM and the conclusions are drawn upon FoM values.

$$FoM = \frac{\Gamma}{FWHM_\gamma + FWHM_n} \quad (10)$$

3. Results and discussion

3.1. Conventional PSD versus DBQC

In this section, the 3D plot of the PSD value has been shown as a function of LIR parameter with the intensity as the third dimension to compare the conventional and DBQC methods. As it can be seen in Fig. 6, (1) the DBQC method has the NGD capability, and, (2) in a low-energy region, the DBQC can be used more efficiently. The latter

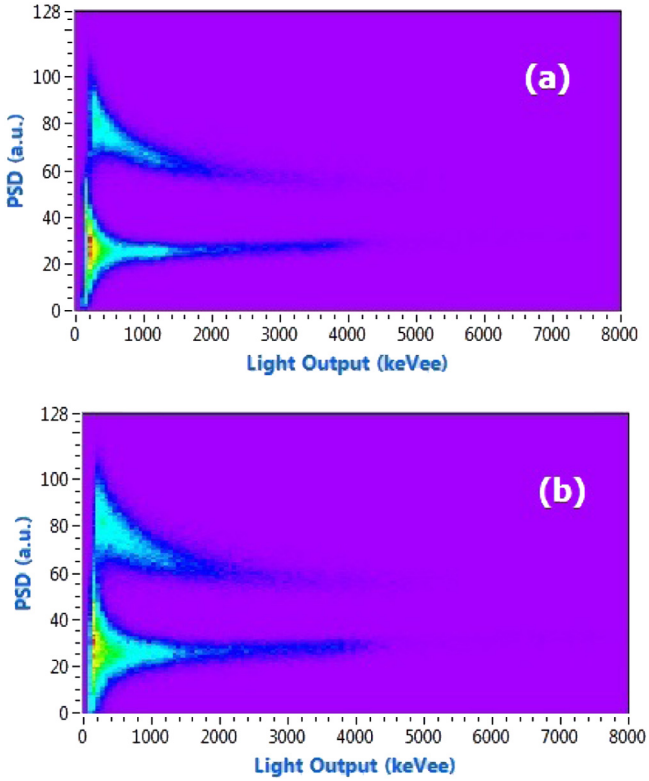

Fig. 6. The 3D plot of the NGD undertaken with liquid scintillator when exposed to ^{241}Am-Be neutron source, using: (a) DBQC and (b) conventional NGD.

is obvious in Fig. 6 as the neutron and gamma ray peaks have been well-separated and became narrower.

Both the type and number of pulse features are important in DBQC method. In this study, two different modes have been considered for the NGD: F7 and F4, in which 7 and 4 different features have been taken into account. In F4 mode, the selected features are LRI, SRI, DRI and PSD. Since, the NGD is more enhanced at the end region of the detector pulse, the more sensitive features at this region have been selected in F4 mode. The variation of three different parameters, η, σ and K has been investigated for both F4 and F7 modes.

3.2. Variation of FoM against η and σ change in F4 and K=5 (K5) mode

The variation of FoM versus η and σ in F4 and K5 mode has been shown in Figs. 7 and 8. Fig. 7 shows that the variation of FoM against σ for different η values is about 7%. The data confirm that the FoM value at each η value is independent of σ, no matter the FoM increases with η. As seen in Fig. 8, the variation of FoM against η at different σ exhibits an increasing trend (+30%). It confirms that the variation of η has more influence on the FoM than on σ.

3.3. Variation of FoM against η and σ change in F7 and K5 mode

The variation of FoM against σ and η values in F7 and K5 mode have been shown in Figs. 9 and 10. The effect of σ on the FoM for different η values has been shown in Fig. 9, whilst Fig. 10 represents the FoM against η for different σ values. Here, the FoM varies up to 10% which is similar to F4, however, the range of variation in F7 mode is smaller compared to F4, for different η values. Fig. 10 shows that the variation of FoM against η is about 20% for a different σ. Therefore, one may conclude that η has more influence on the FoM compared to σ.

Similarly, in this case, the variation range of FoM in F7 is lower than F4 mode. The reason is due to the number of involving parameters that

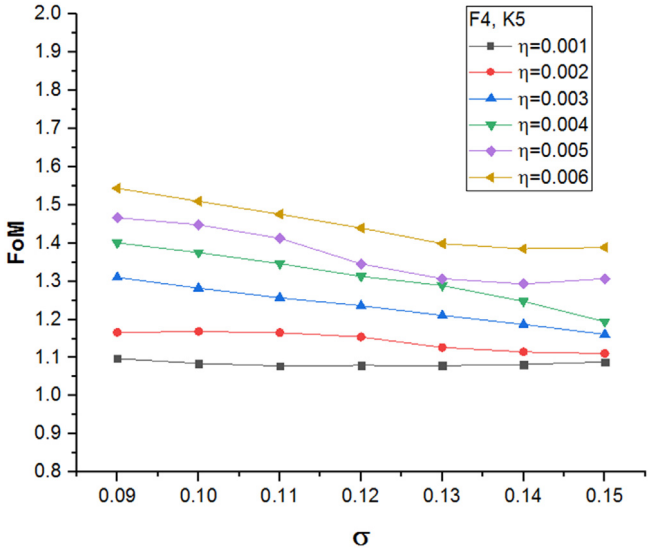

Fig. 7. The Variation of FoM versus σ for different η values in F4 and K5 mode.

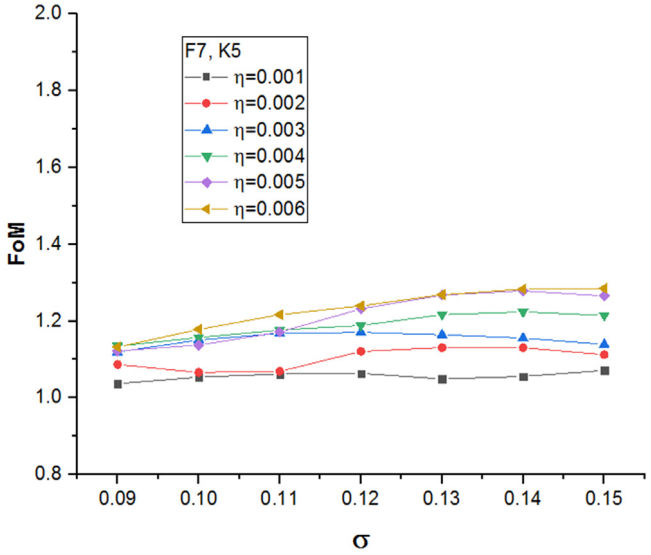

Fig. 9. The Variation of FoM versus σ for different η values in F7 and K5 mode.

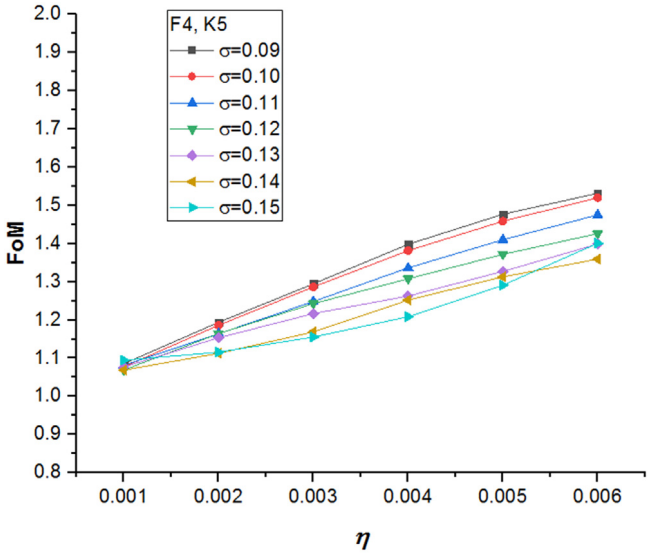

Fig. 8. Variation of FoM versus η for different σ values in F4 and K5 mode.

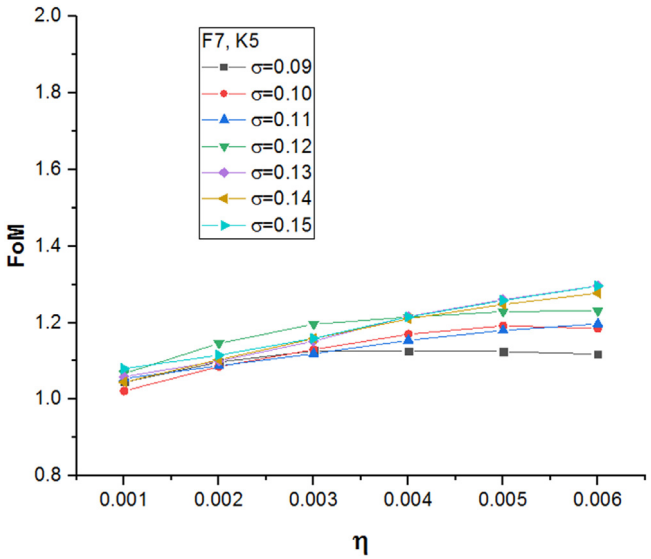

Fig. 10. Variation of FoM versus η for different σ values in F7 and K5 mode.

restrict the paths of data points towards the potential minimum which is larger in F7 compared to F4 mode. It causes the motion of data points to the minimum to become more difficult in F7 compared to F4 mode which consequently decreases the FoM.

3.4. Variation of FoM against the average η and σ changes for different K values

In F4 mode, as shown in Fig. 11, the FoM averaged over different η values does not change considerably and may be regarded as constant. However, the FoM increases with increasing K, so that, the FoM at K=8 is 40% higher than at K=1. In Fig. 12, it is seen that the FoM averaged over σ increases with η so does the FoM slope with increasing K. In F7 mode, the variations of FoM averaged over both η and σ as functions of σ and η exhibit different behavior compared to F4 (Figs. 13 and 14). The increasing slope in F7 is clearly larger than in F4. Overall, one may conclude that the FoM at a given σ, η and K values is larger in F4 compared to F7 mode.

4. Conclusions

In this study, the NGD has been performed on BC501 liquid scintillator pulses using discrimination based on quantum clustering (DBQC) method. Different parameters of DBQC method have been investigated in order to study the variation of the NGD quality factor, FoM. In this method, 7 different features have been extracted as LRI, SRI, DRI, PSD, PW, MV and DI. Two modes, F4 and F7, have been introduced, in which 4 and 7 different features are used for the DNGD, respectively. Moreover, the effects of σ, η and K values on FoM have been studied in details.

In F4 mode, the variation of FoM value is less than 7% which remains almost constant as σ changes for different η values. However, the FoM value exhibits an increasing trend when it is plotted against η for different σ's, so that the FoM at maximum η value is 30% higher than for minimum η value. It confirms that the NGD using DBQC method is almost independent of σ value in F4 mode but it is very sensitive to η.

In F7 mode, similar to F4, FoM value when plotted against σ for different η's remains almost constant. Whilst, FoM increases with η

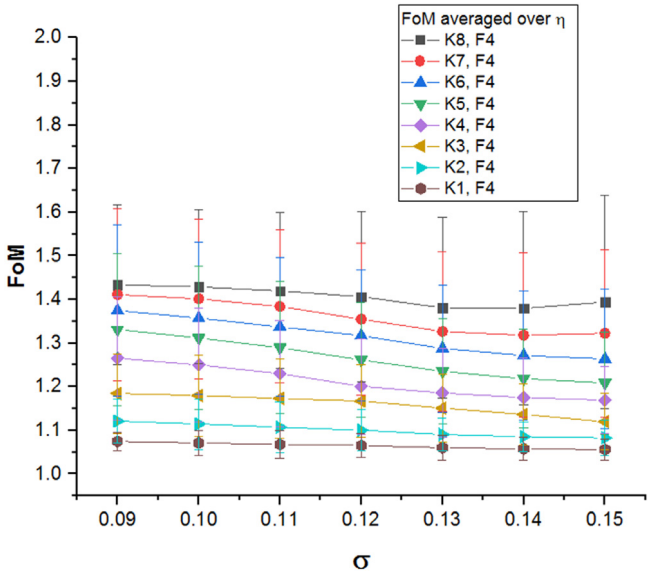

Fig. 11. Variation of average FoM against σ for different η and K values in F4 mode.

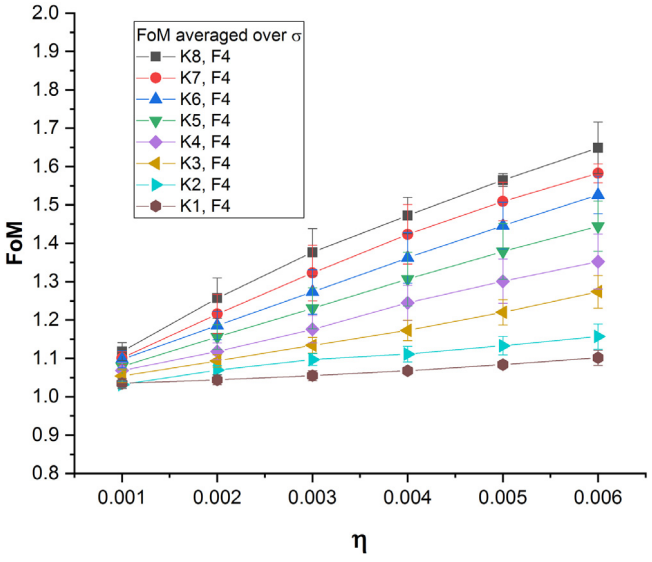

Fig. 12. Variation of average FoM against η for different σ and K values in F4 mode.

for different σ's. Therefore, in F7 mode, the variation of η has more influence on FoM compared to σ.

The measurement results show that FoM in F7 mode is smaller than in F4 mode, which can be interpreted from different points of view: (1) When the number of features increases, the data points become entangled, hence; their motion to the CC's becomes difficult, which causes a poor neutron and gamma-ray clustering. (2) In DBQC, having extracted the important features, the feature selection is of high importance, because if the appropriate features are not selected, the suitable NGD cannot be performed. The studies on different features show that PW, MV and DI features are not only unimportant to the NGD procedure, but also they degrade FoM. One may conclude that only those features should be selected which are more influenced by neutron and gamma-ray pulse difference.

It can be seen that the FoM increases with K, however, in the expense of the DBQC processing time. Therefore, if the NGD is undertaken in off-line mode, FoM value can be increased. FoM value presented in this study is larger compared to other numerical methods previously

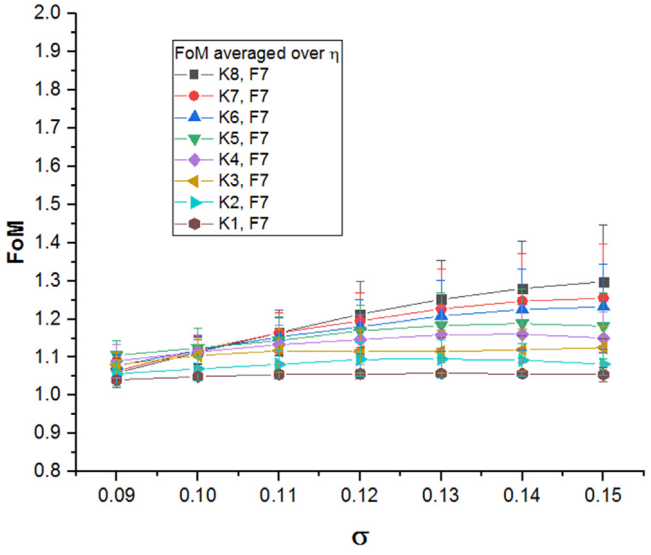

Fig. 13. Variation of average FoM against σ for different η and K values in F7 mode.

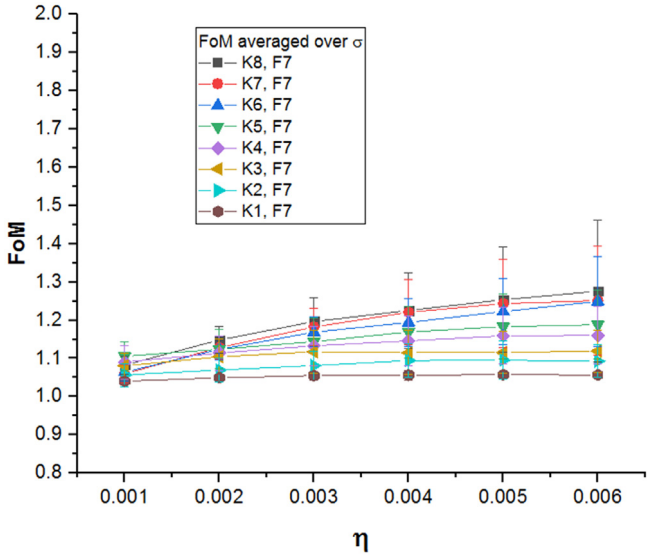

Fig. 14. Variation of average FoM against η for different σ and K values in F7 mode.

Table 1
The comparison among different NGD methods.

Reference	Energy Bias (keVee)	Method	FoM
Ref. [13]	50–200	DFT	0.7
Ref. [13]	200–1400	DFT	1.3
Ref. [12]	200	CIM	1.18
Ref. [12]	200	FGAM	1.14
Ref. [12]	200	WPTM	1.35
Ref. [12]	200	DFTM	1.49
This study	100	DBQC	up to 1.6

discussed in the literature, which confirms that the DBQC is more efficient when compared with CIM, FGAM, WPTM, DFTM and DFT (Table 1).

In this research, a 500 MS/s sampling rate with a 14-bit resolution digitizer has been used. Since DBQC can improve FoM, one may expect that an appropriate FoM can be achieved with a lower sampling rate normally provided by digitizers of a medium frequency.

Besides, the consumption power, computation cost and complexities are considerably reduced, which are being investigated by authors.

Acknowledgments

We would like to thank Dr. V. Doust-Mohammadi and Dr. N. Abbasi for very fruitful discussion and help.

References

[1] G.F. Knoll, Radiation Detection and Measurement, John Wiley and Sons, 2010.
[2] T. Nakamura, T. Nunomiya, H. Yashima, S. Yonai, Overview of recent experimental works on high energy neutron shielding, Prog. Nucl. Energy 44 (2004) 85–187.
[3] N. Divani-Vais, E. Bayat, M.M. Firoozabadi, N. Ghal-Eh, Neutron-gamma discrimination with UGAB scintillator using zero-crossing method, Radiat. Prot. Dosim. 154 (2012) 381–384.
[4] N.V. Kornilov, V.A. Khriatchkov, M. Dunaev, A.B. Kagalenko, N.N. Semenova, V.G. Demenkov, A.J.M. Plompen, Neutron spectroscopy with fast waveform digitizer, Nucl. Instrum. Methods A497 (2003) 467–478.
[5] C. Hellesen, M. Skiba, G. Ericsson, E.A. Sundn, F. Binda, S. Conroy, J. Eriksson, M. Weiszog, Impact of digitization for timing and pulse shape analysis of scintillator detector signals, Nucl. Instrum. Methods A720 (2013) 135–140.
[6] D. Cester, M. Lunardon, G. Nebbia, L. Stevanato, G. Viesti, S. Petrucci, C. Tintori, Pulse shape discrimination with fast digitizers, Nucl. Instrum. Methods A748 (2014) 33–38.
[7] M. Flaska, M. Faisal, D.D. Wentzlok, S.A. Pozzi, Influence of sampling properties of fast-waveform digitizers on neutron gamma-ray, pulse-shape discrimination for organic scintillation detectors, Nucl. Instrum. Methods A729 (2013) 456–462.
[8] S. Jamili, E. Bayat, H. Afarideh, F.A. Davani, N. Ghal-Eh, Digital neutron-gamma discrimination in a wide energy range using pulse reconstruction method, Radiat. Phys. Chem. 109 (2015) 13–16.
[9] S. Jamili, E. Bayat, N. Ghal-Eh, Digital neutron-gamma discrimination with scintillators: An innovative approach, Radiat. Phys. Chem. 132 (2017) 13–15.
[10] D. Takaku, T. Oishi, M. Baba, Development of neutron-gamma discrimination technique using pattern-recognition method with digital signal processing, Prog. Nucl. Sci. Technol. 1 (2011) 210–213.
[11] M. Amiri, J. Čechák, Z. Matěj, Discrimination of neutron and photon signals using time and frequency domain data, GRANT J. (2012).
[12] M.J. Safari, F.A. Davani, H. Afarideh, S. Jamili, E. Bayat, Discrete fourier transform method for discrimination of digital scintillation pulses in mixed neutron-gamma fields, IEEE Trans. Nucl. Sci. 63 (2016) 325–332.
[13] M. Nakhostin, Digital discrimination of neutrons and γ-rays in liquid scintillation detectors by using low sampling frequency ADCs, Nucl. Instrum. Methods A916 (2019) 66–70.
[14] S. Gou, X. Zhuang, L. Jiao, SAR image segmentation using quantum clonal selection clustering, in: Synthetic Aperture Radar, APSAR 2009, 2nd Asian-Pacific Conference, 2009, pp. 817–820.
[15] M. Weinstein, A. Heifetz, R. Klann, Detection of nuclear sources in search survey using dynamic quantum clustering of gamma-ray spectral data, Eur. Phys. J. Plus 129 (2014) 239.
[16] Y. Li, Y. Wang, Y. Wang, L. Jiao, Y. Liu, Quantum clustering using kernel entropy component analysis, Neurocomputing 202 (2016) 36–48.
[17] S.S. Kim, H.J. Choi, K.C. Kwak, Knowledge extraction and representation using quantum mechanics and intelligent models, Expert Syst. Appl. 39 (2012) 3572–3581.
[18] N. Hamdi, K. Auhmani, M.M. Hassani, Quantum clustering-based feature subset selection for mammographic image classification, Intl. J. Comput. Sci. Inform. Technol. 7 (2015) 127.
[19] M. Weinstein, D. Horn, Dynamic quantum clustering: A method for visual exploration of structures in data, Phys. Rev. E 80 (2009) 066117.
[20] H.H. Knox, T.G. Miller, A technique for determining bias settings for organic scintillators, Nucl. Instrum. Methods 101 (1972) 519–525.
[21] W.H. Press, S.A. Teuklosky, W.T. Vetterling, B.P. Flannery, Numerical Recipes, Cambridge University Press, 1992.
[22] J. Barzilai, J.M. Borwein, Two-point step size gradient methods, IMA J. Numer. Anal. 8 (1988) 141–148.
[23] D. Babichev, F. Bach, Constant step size stochastic gradient descent for probabilistic modeling, 2018, ArXiv preprint arXiv:1804.05567.